Wavelength-Dependent Photodissociation of $[Fe(bpy)_3 \cdot (CH_3OH)_n]^{2+}$ Clusters, $n = 2-6$, Triggered by Excitation of the Metal-to-Ligand Charge-Transfer Transition

Thomas G. Spence, Thomas D. Burns,† G. Brody Guckenberger, V,‡ and Lynmarie A. Posey*

Department of Chemistry, Vanderbilt University, Box 1822, Station B, Nashville, Tennessee 37235

Received: September 24, 1996; In Final Form: November 20, 1996⊗

This paper reports the first investigation of the energetics of charge transfer in a coordination complex containing a *divalent* transition-metal ion as a function of the extent of solvation and provides a detailed description of the first instrument designed for spectroscopic characterization of gas-phase ions and clusters produced by electrospray ionization. Metal-to-ligand charge transfer (MLCT) is probed by laser photofragmentation mass spectrometry in clusters of the complex tris(2,2′-bipyridyl)iron(II), $[Fe(bpy)_3]^{2+}$, with methanol prepared by electrospray ionization. Excitation of the MLCT transition in $[Fe(bpy)_3]^{2+}$ triggers evaporation of methanol solvent molecules from these clusters, permitting indirect detection of absorption. Measurement of ion beam depletion and/or production of charged photofragments as a function of photon energy yields the red edge of the MLCT band for $[Fe(bpy)_3 \cdot (CH_3OH)_n]^{2+}$ clusters, $n = 2-6$. Increasing the number of methanol molecules in the clusters shifts the onset of the MLCT band to lower energies, reflecting preferential solvation of the MLCT excited state of $[Fe(bpy)_3]^{2+}$ relative to its ground state. A measurable fraction of mass-selected $[Fe(bpy)_3 \cdot (CH_3OH)_n]^{2+}$ clusters also lose methanol molecules through metastable decomposition between primary mass selection and secondary mass analysis. Application of the evaporative ensemble model with RRK rate constants for metastable decomposition permits estimation of sequential methanol binding energies and internal temperatures for $[Fe(bpy)_3 \cdot (CH_3OH)_n]^{2+}$ clusters prepared by electrospray ionization.

I. Introduction

The chemical reactivity and dynamics of ions in the condensed phase are strongly influenced by the surrounding solvent environment.[1] For example, comparison of reaction rates observed in the gas phase with those observed under bulk conditions for simple nucleophilic displacement reactions reveals the dramatic effect that surrounding solvent molecules can have on the dynamics of chemical reactions.[2] In the condensed phase, it is often difficult to distinguish the influence of individual solvent molecules in the primary solvent shell[3] from that of the bulk solvent. However, recent studies of weakly bound, gas-phase clusters consisting of an ion and neutral molecules have promoted clusters as simplified models for investigating the interactions between ionic solutes and neutral solvent molecules[4,5] because clusters offer systematic control over both the extent of solvation and the identity of the solvent. In this paper, we report the first study using gas-phase clusters to investigate the influence of sequential solvation on the energetics of photoinitiated charge transfer in a coordination complex containing a divalent transition-metal ion. A unique technical aspect of this work is the coupling of electrospray ionization (ESI) to prepare clusters with laser photofragmentation mass spectrometry to probe the electronic structure of the cluster chromophore.

Despite the importance of the +2 oxidation state of transition metal ions in solution chemistry, *doubly charged* transition-metal ions and clusters containing these ions have been largely ignored in gas-phase studies.[6] Most of the work on dipositive transition-metal ions in the gas phase has involved reactions of single metal ions produced by laser vaporization with small hydrocarbons. In 1986, Weisshaar and co-workers[7] reported the first study of this type, an investigation of the reactivity of Ti^{2+} with small alkanes. Subsequently, Freiser and co-workers[8−11] examined the gas-phase reactivity of Ta^{2+}, Zr^{2+}, Y^{2+}, V^{2+}, and Nb^{2+} with several small hydrocarbons. A common feature of the doubly charged transition-metal ions prepared by laser vaporization for reaction studies was the relatively low second ionization potential ($\leq$15.5 eV), which may be an inherent limitation of laser vaporization as a method of preparing doubly charged transition-metal ions. With the exception of electrospray ionization,[12] other ionization/volatilization techniques commonly employed in analytical mass spectrometry have proven even less successful as general methods for generating multiply charged gas-phase transition-metal ions. Stace and co-workers[13,14] recently reported a possible alternative to electrospray ionization for generating clusters containing doubly charged transition-metal ions. They prepared $Mg^{2+} \cdot (solvent)_n$ clusters by passing neutral solvent clusters through Mg vapor and then ionizing clusters which had incorporated a metal atom by electron impact; however, this technique has not yet been demonstrated for transition metals.

Electrospray ionization transfers transition-metal ions and transition-metal ion complexes, which are already multiply-charged in solution, to the gas phase without reduction as shown initially by Kebarle and co-workers[15−17] and subsequently by others.[18−20] Kebarle and co-workers found that ESI of solutions containing divalent transition and alkaline earth metal ions produced $M^{2+} \cdot L_n$ clusters, where M^{2+} was the metal ion and L was a ligand such as water, dimethyl sulfoxide, dimethylformamide, or pyrazine that was present in solution. They investigated ion-hydration equilibria[15] by passing $M^{2+} \cdot (H_2O)_n$ clusters generated by ESI through an interface cell containing a controlled partial pressure of water vapor and then measuring the resulting distribution of clusters, which permitted determination of sequential free energies and enthalpies of hydration. As part of the same study, Kebarle and co-workers[15] also began

* To whom correspondence should be addressed. E-mail: poseyla@ctrvax.vanderbilt.edu.

† Current address: Department of Chemistry, Florida Southern College, Lakeland, FL 33801.

‡ Current address: Department of Chemistry, University of Florida, Gainesville, FL 32611.

⊗ Abstract published in *Advance ACS Abstracts,* January 1, 1997.

S1089-5639(96)02939-8 CCC: $14.00

to explore stabilization of the +2 charge in $M^{2+}\cdot L_n$ clusters by monitoring the competition between ligand dissociation and metal ion reduction in collisionally-activated clusters. This work provided the first glimpse of the tremendous potential of ESI mass spectrometry as a tool for studying the detailed interactions between divalent transition-metal ions and individual solvent molecules in the absence of the bulk solvent. It also opened the possibility of studying these species spectroscopically.

Laser photofragmentation mass spectrometry has been applied previously to measure the electronic and vibrational spectra of clusters containing singly charged metal ions. For example, Brucat and co-workers have obtained vibrationally resolved photofragmentation spectra for several systems consisting of a singly charged transition-metal ion clustered with a rare gas atom,[21−25] CO_2 molecule,[26−28] or H_2O molecule[29] when metal ion-based electronic transitions were excited. Duncan and co-workers have used cluster photofragmentation to collect vibronic spectra of $Mg^+\cdot$rare gas,[30,31] $Mg^+\cdot H_2O$,[32,33] and $Mg^+\cdot CO_2$ clusters.[34] They also located a charge-transfer absorption band for $Ag^+\cdot$benzene clusters[35] by monitoring the benzene cation produced by photoinitiated transfer of an electron from the benzene ligand to Ag^+. Farrar and co-workers[36,37] have collected the photofragmentation spectra of $Sr^+\cdot(NH_3)_n$ clusters, $n = 1-4$. New features appeared in the spectra of clusters containing three or four NH_3 molecules, which were attributed to charge transfer from the Sr^+ ion to the NH_3 "solvent" to form an ammoniated electron, analogous to that observed in the condensed phase. Cluster size-dependent infrared vibrational predissociation spectra of $Cs^+\cdot(CH_3OH)_n$ and $Na^+\cdot(CH_3OH)_n$ clusters measured by Lisy and co-workers[38−40] have provided evidence of completion of the primary solvent shell, which was supported by molecular dynamics simulations.

These studies have shown that analysis of photofragmentation spectra can provide information on the structure of gas-phase clusters, ground-state binding energies between ions and associated neutral atoms or molecules, and shifts in the absorption bands. In some instances, the appearance of new absorption features attributed to the presence of the surrounding solvent environment have even been observed.[36,37,41] Laser photofragmentation mass spectrometry has become the detection method of choice in ionic cluster studies because it offers a sensitive, although indirect measure of absorption by gas-phase ions whose low concentrations preclude direct measurement of the attenuation of light passing through a sample. It should be noted, however, that the following assumptions are inherent in using laser photofragmentation action spectra as measures of cluster absorption: the photon absorbed has sufficient energy to induce photodissociation, sufficient time is allowed for photodissociation to occur, and radiative decay pathways do not compete appreciably with the photodissociation process.

In this paper, we report one of the first applications of ESI to prepare clusters containing divalent transition-metal ions for subsequent study via laser photofragmentation spectroscopy.[42] The target transition-metal ion complex, tris(2,2′-bipyridyl)-iron(II), $[Fe(bpy)_3]^{2+}$ (bpy = bipyridyl), exhibits a strong metal-to-ligand charge-transfer (MLCT) transition in solution. This absorption band has a maximum at 19 160 cm^{-1} in methanol ($\epsilon = 8740\ M^{-1}\ cm^{-1}$).[43] The MLCT transition

$$[Fe^{II}(bpy)_3]^{2+} \xrightarrow{h\nu} [Fe^{III}(bpy^-)(bpy)_2]^{2+} \quad (1)$$

is formally classified as a $d_{t_{2g}} \rightarrow \pi^*$ transition. In contrast with the analogous ruthenium complex $[Ru(bpy)_3]^{2+}$, $[Fe(bpy)_3]^{2+}$ exhibits no luminescence from excited MLCT states due to very efficient nonradiative decay paths provided by triplet and quintet ligand-field states,[44] making this system a good choice for indirect detection of absorption via photofragmentation. Excitation of this MLCT transition in clusters

$$\{[Fe^{II}(bpy)_3]\cdot(CH_3OH)_n\}^{2+} \xrightarrow{h\nu} \{[Fe^{III}(bpy^-)(bpy)_2]^*(CH_3OH)_n\}^{2+} \quad (2)$$

triggers the evaporation of neutral methanol solvent molecules as the system relaxes,

$$\{[Fe^{III}(bpy^-)(bpy)_2]^*(CH_3OH)_n\}^{2+} \rightarrow (n-m)CH_3OH + \{[Fe^{II}(bpy)_3]\cdot(CH_3OH)_m\}^{2+} \quad (3)$$

We have measured the wavelength-dependent photodissociation yield between 530 and 600 nm for mass-selected $[Fe(bpy)_3\cdot(CH_3OH)_n]^{2+}$ clusters, $n = 2-6$. The resulting photodissociation action spectra reflect the onset of the MLCT absorption band as a function of cluster size. We have also used metastable decomposition data to estimate sequential binding energies and internal temperatures in the context of the evaporative ensemble model for $[Fe(bpy)_3\cdot(CH_3OH)_n]^{2+}$ clusters prepared by ESI.

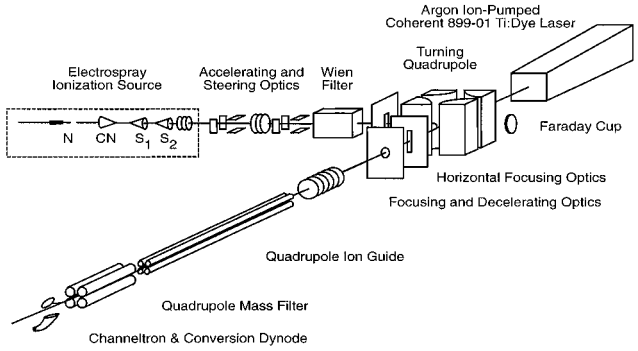

Figure 1. Schematic diagram of the tandem mass spectrometer with electrospray ionization source. Key components of the electrospray ionization source are labeled as follows: N = needle, CN = conical nozzle, S_1 = skimmer 1, and S_2 = skimmer 2.

II. Experimental Section

A. Overview. Experiments are performed using the laser-interfaced tandem mass spectrometer illustrated in Figure 1. Briefly, clusters of the transition-metal ion complex $[Fe(bpy)_3]^{2+}$ with methanol are prepared by electrospray ionization. The Wien filter in the first stage of the tandem mass spectrometer selects a specific cluster size from the distribution generated by ESI. The mass-selected parent ion beam is then deflected 90° by an electrostatic turning quadrupole, refocused, and merged with the output from a tunable, continuous wave (CW) dye laser. The ion and laser beams copropagate through electrostatic decelerating optics, a radio-frequency (rf) quadrupole ion guide, and a quadrupole mass filter. The quadrupole mass filter in the second stage of the tandem mass spectrometer resolves the parent ion beam from charged photoproducts before detection with a conversion dynode and a Channeltron electron multiplier.

B. Electrospray Ionization. The electrospray ionization source (Vestec Corp. Model E200) is described in detail elsewhere.[45] Key components of the ESI source are shown in Figure 1. Since ESI is not typically used to generate clusters, the discussion of the ESI source will focus on the experimental conditions employed to produce clusters. Clusters of composition $[Fe(bpy)_3\cdot(CH_3OH)_n]^{2+}$ are produced by ESI of a dilute solution of $Fe(bpy)_3(ClO_4)_2$ (GFS Chemicals) in methanol (Fisher, Certified A.C.S. grade). A mechanical syringe pump

(Harvard Apparatus Classic Microliter syringe pump) delivers solution through a fused silica capillary to the electrospray needle (0.125 mm i.d., 90° tip bevel). Optimum ion signal intensity and stability are obtained with a 1.5×10^{-4} M solution of $Fe(bpy)_3(ClO_4)_2$ in methanol, delivered to the needle tip at a rate of 1.4 μL min^{-1}. The electrospray needle (N in Figure 1) is biased at 2.0−2.6 kV with respect to a conical nozzle (CN) having a 0.6 mm aperture located 2−3 mm from the needle tip. The electrospray current, typically 0.20−0.25 μA, is monitored at the conical nozzle.

Clusters of the ionic analyte with the electrospray solvent naturally form in ESI. Electrospray ionization sources designed for analytical applications typically use either heat[45,46] or countercurrent flow of dry nitrogen[12,47] to desolvate the analyte ions. The Vestec source heats the first differential pumping stage located between the conical nozzle (CN) and first skimmer (S_1) to desolvate analyte ions. The desolvation chamber of the ion source is maintained at 36 °C to minimize desolvation of the transition-metal ion complex, while preventing the methanol from freezing in the conical nozzle aperture.

C. Vacuum System for Electrospray Ionization Source and Tandem Mass Spectrometer. Ions formed at atmospheric pressure in the electrospray ionization chamber first pass through the conical nozzle and then through two skimmers before entering the mass spectrometer. The skimmers (S_1 and S_2 in Figure 1) have 0.8 and 1.0 mm diameter apertures, respectively. The nozzle and the skimmers define the two stages of differential pumping required to reach a suitable pressure for carrying out mass spectrometry. A mechanical pump (Fisher Maxima D30A, 760 L min^{-1}) maintains a pressure of 2−3 Torr in the first stage of differential pumping in the ESI source located between the conical nozzle and first skimmer. The pressure in the second differential pumping stage located between the two skimmers is held at 150 mTorr by a second mechanical pump (Fisher Maxima D16A, 400 L min^{-1}).

Ions travel through the first two stages of differential pumping in the ESI source under the influence of continuum flow and an applied electric field. Knudsen numbers[48] indicate continuum flow through the nozzle and the first skimmer. Consequently, some rotational cooling is anticipated, although vibrational cooling remains inefficient. By the time the ions pass through the second skimmer (S_2), the background pressure is reduced to the point where flow is intermediate between the continuum and molecular regimes. Ions do not acquire significant kinetic energy from the applied electric fields until they exit from the source through the second skimmer because the gas density is sufficiently high that ions collide with background gas before they are fully accelerated by the electric field. Retardation analysis of the ion beam verifies that its kinetic energy is determined by the potential difference with respect to the second skimmer.[49]

The vacuum chamber for the tandem mass spectrometer consists of three differentially-pumped stages, each of which is evacuated by an oil diffusion pump. When the ESI source is operating, the first stage containing the acceleration lenses, deflectors, and Wien filter is maintained at 5×10^{-6} Torr by an Edwards 250 Diffstak (2000 L s^{-1}). The second stage, which houses an electrostatic turning quadrupole, and the third stage, which contains the quadrupole ion guide and quadrupole mass filter, are each evacuated by an Edwards 160 Diffstaks (700 L s^{-1}) to reach operating pressures of 1×10^{-6} and 3×10^{-8} Torr, respectively.

D. Primary Mass Selection. Upon exiting the ESI source, cluster ions are focused and accelerated by an electrostatic lens stack into a Wien filter (Colutron Research, Model 600B, magnetic field strength 3000 G). All ions exiting the ESI source are accelerated through the same potential (typically 160 V), resulting in different velocities for cluster ions having different mass-to-charge ratios (*m/z*). The Wien filter[50,51] uses perpendicular electric and magnetic fields to separate ions with different velocities. The electric field is tuned so that only those cluster ions with velocities corresponding to a specific *m/z* pass through the Wien filter undeflected and subsequently through a 2.5 mm aperture located 44 cm from the Wien filter exit.

The ion beam emerging from the Wien filter can either be monitored by measuring the current from a Faraday cup or deflected 90° and merged with a CW laser beam by an electrostatic turning quadrupole.[52,53] When the electric and magnetic fields of the Wien filter are turned off to allow all ions to pass through undeflected, ion currents measured at the Faraday cup range from 0.03 to 0.05 nA. Following deflection by the turning quadrupole, the ion current measured ranges from 0.01 to 0.02 nA. A line focus aperture lens[54] focuses ions exiting the turning quadrupole in the horizontal plane to correct for the astigmatism of the turning quadrupole, while allowing ions deflected by the Wien filter to continue to disperse in the vertical plane. Ions not deflected by the Wien filter are then focused and decelerated by a cylindrical lens stack before entering a quadrupole ion guide (80.0 cm long, 0.95 cm diameter rods) powered by a commercial rf oscillator (Extrel QCRF1, 100 W, 1.2 MHz). The parabolic effective potential established in the quadrupole ion guide confines the ion beam radially to maximize overlap between the ions and the laser beam.[55]

E. Laser System. Ions in the mass-selected beam are excited as they traverse the decelerating optics and the ion guide by either a single line from a CW argon ion laser (Coherent Innova 420, 20 W multiline output) or the tunable output from an argon ion-pumped ring dye laser (Coherent 899-01 Ti:dye). Selection of a single line from the multiline output of the argon ion laser is accomplished using extracavity prisms and a slit.[56] The tunable ring dye laser operates at wavelengths ranging from 530 to 600 nm using pyrromethene 556, rhodamine 110, and rhodamine 6G dyes (Exciton). A Burleigh Wavemeter Jr. monitors the output wavelength of the dye laser.

The laser beam is chopped at 210 Hz (Stanford Research Systems SR540 optical chopper), allowing for acquisition of both laser-on and laser-off ion signals. The $[Fe(bpy)_3 \cdot (CH_3OH)_n]^{2+}$ clusters spend from 118 μs for $n = 2$ to 130 μs for $n = 6$ in the laser interaction region, ensuring that each ion experiences only one laser-on or laser-off cycle. The laser beam passes through a Galilean telescope consisting of a −200 mm focal length (fl) lens and a 100 mm fl lens. Slight detuning of the telescope from the beam collimation geometry results in a measured focal length of 1.5 m. The laser beam has an average diameter over the laser/ion beam interaction region of 0.75 mm. The focal point is located inside the quadrupole mass filter.

A half-wave plate located before a Glan laser polarizer permits adjustment of the power of the argon ion or dye laser beam while maintaining fixed linear polarization. Depletion of the parent ion beam and production of photoproduct ions show a linear dependence over the range of powers used. Typical laser powers of 100−400 mW (23−91 W cm^{-2}) monitored at the exit of the mass spectrometer (Ophir 10A thermopile detector, DGX display) result in 3.8−15% depletion of $[Fe(bpy)_3 \cdot (CH_3OH)_6]^{2+}$ clusters at 530 nm, where the strongest cluster absorption is observed with dye laser excitation. By using laser fluences which keep the percent depletion of the mass-selected parent beam below 15%, saturation of the strong MLCT transition in the $[Fe(bpy)_3]^{2+}$ complex ($\epsilon = 8740$ M^{-1} cm^{-1} at $\lambda_{max} = 522$ nm in methanol solution)[43] is avoided,

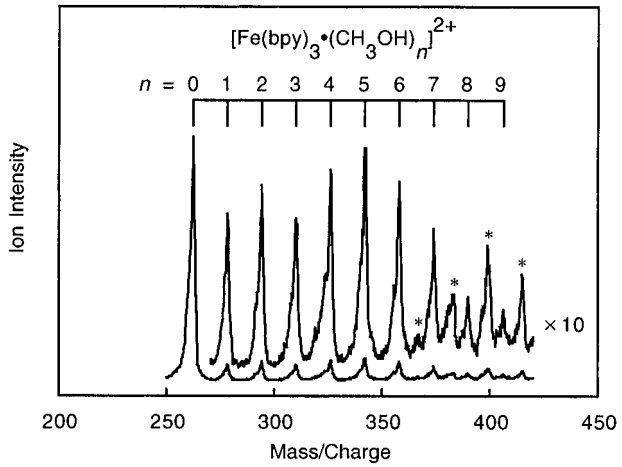

Figure 2. Mass spectrum generated by electrospray ionization of 1.5×10^{-4} M $Fe(bpy)_3(ClO_4)_2$ in methanol. The unsolvated $[Fe(bpy)_3]^{2+}$ ion appears as an intense peak at $m/z = 262.2$ and is followed by a progression of peaks corresponding to $[Fe(bpy)_3 \cdot (CH_3OH)_n]^{2+}$ clusters. A second progression designated by asterisks, which is attributed to the mixed solvent clusters $[Fe(bpy)_3 \cdot (CH_3OH)_n \cdot (H_2O)]^{2+}$, grows in for $n \geq 6$.

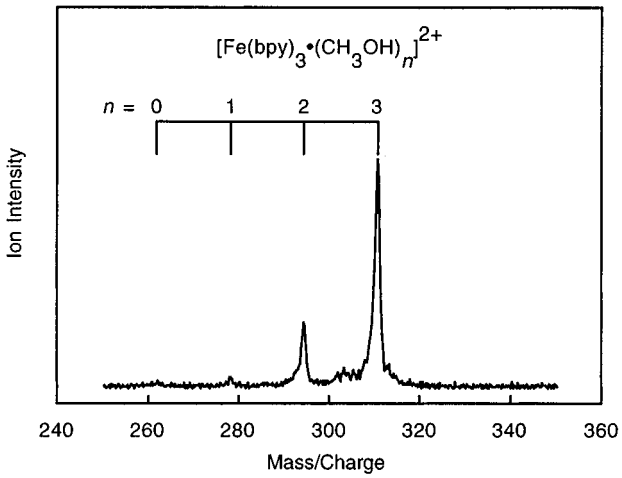

Figure 3. Mass spectrum resolved by the quadrupole mass filter following primary mass selection of $[Fe(bpy)_3 \cdot (CH_3OH)_3]^{2+}$ clusters with the Wien filter. Metastable decomposition of mass-selected $[Fe(bpy)_3 \cdot (CH_3OH)_3]^{2+}$ clusters as they travel from the Wien filter to the quadrupole mass filter produces the smaller clusters observed.

and absorption by photoproducts triggering subsequent photofragmentation is negligible.

F. Detection of Charged Photoproducts and Attenuation of Parent Ion Beam. Photofragment and parent cluster ions are resolved by a quadrupole mass filter (Extrel EXM-340 system, 1.59 cm diameter, 22 cm long rods, 200 W, 1.2 MHz, *m/z* range 1−450 amu) after exiting the ion guide. The ions are then detected using a conversion dynode and an ion-counting Channeltron particle multiplier (Galileo Electro-Optics Model 4870). Current from the detector passes through three stages of amplification (Stanford Research Systems SR440 quad preamplifier, 5× amplification/stage). Single ion pulses are subsequently scored by a two-channel gated photon counter (Stanford Research Systems SR400) synchronized with the laser beam chopper. With this gated detection scheme, data are collected during the middle 50% of each cycle and stored in separate channels for laser-on and laser-off cycles. Typical ion intensities detected at the Channeltron detector are 2×10^6 ions s^{-1} for the $[Fe(bpy)_3]^{2+}$ ion, and $(1-2) \times 10^3$ ions s^{-1} for the mass-selected $[Fe(bpy)_3 \cdot (CH_3OH)_n]^{2+}$ clusters.

G. Data Acquisition and Instrument Control. Data acquisition and instrument control are managed by a Macintosh IIci through GPIB and serial interfaces. The quadrupole mass filter is swept by a D/A output from a Stanford Research Systems SR245 computer interface module. Mass spectra showing the distribution of ions produced by ESI are obtained by switching off the electric and magnetic fields of the Wien filter and scanning the quadrupole mass filter. Laser-on and laser-off spectra are recorded by the Macintosh IIci as the quadrupole mass filter is swept through a mass range encompassing the parent ion and all photofragment ions.

III. Results and Discussion

A. Electrospray Ionization Mass Spectrometry. The mass spectrum in Figure 2 shows a typical distribution of cluster ions produced by electrospray ionization of $Fe(bpy)_3(ClO_4)_2$ in methanol. The ionic species produced by ESI depend strongly upon the temperature in the desolvation chamber and the electric field strength in the two high-pressure zones of the ESI source. High temperatures promote desolvation, and high electric field strengths increase the kinetic energy of ion collisions with the background gas in the source leading to desolvation and/or fragmentation. Therefore, cluster formation is optimized by keeping the electric field strengths low and operating at the lowest possible desolvation chamber temperature as discussed above. The most intense peak in the mass spectrum at $m/z = 262.2$ corresponds to the unsolvated $[Fe(bpy)_3]^{2+}$ ion. The two peaks anticipated for the $[Fe(bpy)_3]^{2+}$ complex, arising from the two most abundant isotopes of iron, ^{54}Fe (5.82%) and ^{56}Fe (91.18%),[57] are not resolved in the mass spectrum shown in Figure 2. Due to the low signal intensity inherent in this experiment, the resolution of the quadrupole mass filter has been sacrificed to improve ion throughput. The unsolvated ion peak is followed by a less intense progression of $[Fe(bpy)_3 \cdot (CH_3OH)_n]^{2+}$ cluster ion peaks ($n = 1-9$).

Beyond the $[Fe(bpy)_3 \cdot (CH_3OH)_6]^{2+}$ peak in Figure 2, a second series of peaks grows in. These peaks, which are denoted by asterisks, are assigned as $[Fe(bpy)_3 \cdot (CH_3OH)_n \cdot (H_2O)]^{2+}$ clusters. Lisy and co-workers[58] observed an intracluster reaction in $Cs^+ \cdot (CH_3OH)_n$ clusters, which results in elimination of dimethyl ether, $(CH_3)_2O$, from the cluster and retention of H_2O. We ruled out this intracluster reaction as a route for formation of $[Fe(bpy)_3 \cdot (CH_3OH)_n \cdot H_2O]^{2+}$ clusters, when ESI of $Fe(bpy)_3(ClO_4)_2$ dissolved in CH_3OD yielded no $[Fe(bpy)_3 \cdot (CH_3OD)_n \cdot D_2O]^{2+}$ or $[Fe(bpy)_3 \cdot (CH_3OD)_n \cdot HDO]^{2+}$ clusters. Drying the methanol solvent also had no impact on the intensity of water-containing cluster peaks. We found, however, that purging the region between the electrospray needle and nozzle with dry nitrogen reduces the intensity of the water-containing peaks, suggesting that water from the air surrounding the electrospray needle is incorporated in the $[Fe(bpy)_3 \cdot (CH_3OH)_n]^{2+}$ clusters following ESI. Furthermore, purging the ESI region with nitrogen bubbled through methanol enhances the intensity of $[Fe(bpy)_3 \cdot (CH_3OH)_n]^{2+}$ clusters and diminishes the relative intensity of clusters which have incorporated water. Experiments investigating the "pickup" of solvent molecules in the ESI source are reported in a separate paper.[59]

A specific cluster can be selected for further study from the distribution of clusters produced by ESI on the basis of its *m/z* using the Wien filter. Figure 3 shows a mass spectrum obtained with the Wien filter tuned to deflect all ions except $[Fe(bpy)_3 \cdot (CH_3OH)_3]^{2+}$ clusters ($m/z = 310.3$). The $[Fe(bpy)_3 \cdot (CH_3OH)_2]^{2+}$ cluster ions in this spectrum arise from metastable decomposition of $[Fe(bpy)_3 \cdot (CH_3OH)_3]^{2+}$ cluster ions following mass selection by the Wien filter in the approximately 144 μs transit time from the Wien filter to the quadrupole mass filter.

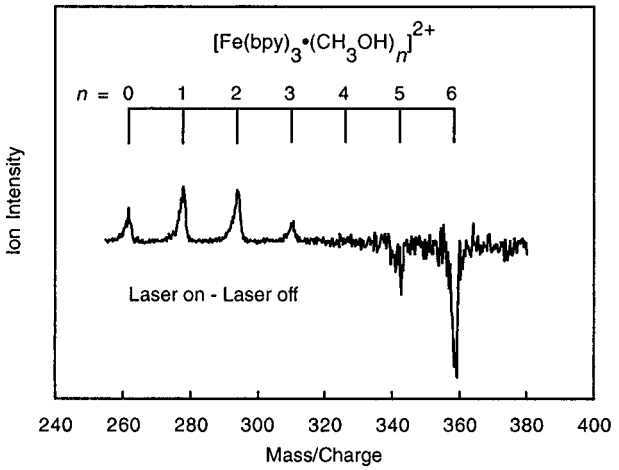

Figure 4. Laser-on−laser-off difference mass spectrum resulting from excitation of $[Fe(bpy)_3 \cdot (CH_3OH)_6]^{2+}$ clusters at 530.0 nm (2.340 eV). The product channels observed correspond to loss of from three to six methanol molecules following excitation.

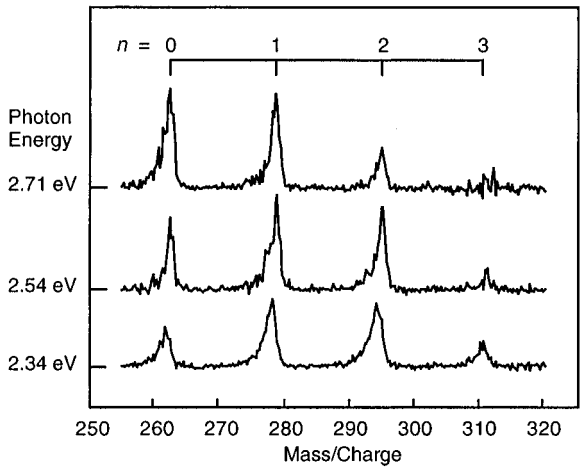

Figure 5. Photoproduct mass spectra observed for $[Fe(bpy)_3 \cdot (CH_3OH)_6]^{2+}$ clusters displayed as a function of photon energy. The intensities of the photoproduct mass spectra were normalized so that the sum of the integrated areas of the photoproduct peaks is the same in each spectrum. The photoproduct distributions shift to smaller clusters with increasing photon energy.

The absence of clusters in this spectrum having larger *m/z* values than the cluster ion selected indicates that the Wien filter resolution is sufficient to resolve neighboring clusters, supporting our contention that the ions at lower *m/z* arise from metastable decay rather than poor resolution of the Wien filter. Given the pressure in the vacuum chamber between the exit of the Wien filter and the entrance to the quadrupole mass filter, a simple hard-sphere collision model predicts that fewer than 2% of the ions experience collisions with background gas molecules. The intensity of the $[Fe(bpy)_3 \cdot (CH_3OH)_2]^{2+}$ cluster ion signal is approximately an order of magnitude greater than expected for dissociation of the cluster ions resulting from collisions with background gas, ruling out collision-induced dissociation (CID) as a major contributor to formation of $[Fe(bpy)_3 \cdot (CH_3OH)_2]^{2+}$. The contribution to the measured photoproduct ion signal from photodissociation of these metastable decay products will be discussed subsequently.

B. Photofragment Ion Distributions. Previously, we have investigated wavelength-dependent photofragmentation of $[Ru(bpy)_3 \cdot (CH_3OH)_n]^{2+}$ and $[Fe(bpy)_3 \cdot (CH_3OH)_n]^{2+}$ clusters using single-line excitation from an argon ion laser.[42] This work demonstrated that the MLCT transition observed in the solution absorption spectra of these complexes is also present in the gas-phase clusters produced by ESI, providing evidence that the same chromophore is found in both phases. In this study, we explore the onset of the lowest energy MLCT transition of $[Fe(bpy)_3]^{2+}$ as the solvent environment surrounding the coordination complex is assembled one solvent molecule at a time. We begin our discussion of laser photofragmentation data by examining the photoproduct distributions generated by excitation of the MLCT transition as a function of cluster size and photon energy.

A typical difference mass spectrum obtained by subtracting a "laser-off" mass spectrum from a "laser-on" mass spectrum is shown in Figure 4 for the mass-selected $[Fe(bpy)_3 \cdot (CH_3OH)_6]^{2+}$ ion excited at 530.0 nm. In this mass spectrum, positive-going peaks correspond to the production of photofragment ions, while the negative-going peaks represent depletion of parent ions. The four photofragments observed correspond to loss of from 3 to 6 solvent molecules following absorption of a photon by the parent cluster ion. Similar distributions of photofragments corresponding to loss of from 3 to 5 and from 3 to 4 methanol molecules are observed for $[Fe(bpy)_3 \cdot (CH_3OH)_5]^{2+}$ and $[Fe(bpy)_3 \cdot (CH_3OH)_4]^{2+}$, respectively. For clusters containing three or fewer methanol molecules, the only photoproduct ion observed is formation of $[Fe(bpy)_3]^{2+}$, which corresponds to loss of all solvent molecules. When the unsolvated $[Fe(bpy)_3]^{2+}$ ion is excited, no evidence of photofragmentation, such as the loss of a bipyridyl ligand, is detected. Therefore, we conclude that there is insufficient energy to dissociate the $[Fe(bpy)_3]^{2+}$ ion on the time scale of the experiment at photon energies of 2.71 eV and below. Absorption by photoproduct ions and subsequent photofragmentation is a common complication in determining photoproduct ion distributions, particularly with strongly absorbing chromophores. However, the photoproduct ion distributions are independent of laser fluence below 91 W cm^{-2}, indicating that absorption by the $[Fe(bpy)_3 \cdot (CH_3OH)_m]^{2+}$ photoproduct ions and subsequent photofragmentation is negligible.

Photofragment ion distributions can be characterized by the average number of solvent molecules lost (or average product cluster size) and width. Figure 5 shows the shift in the photoproduct distribution to smaller cluster sizes as the photon energy increases for $[Fe(bpy)_3 \cdot (CH_3OH)_6]^{2+}$. The traces in this figure are normalized with respect to total area under the photoproduct peaks to facilitate comparison because the total photoproduct ion yield changes with photon energy (section III.D). As the photon energy increases, the photofragment ion distribution becomes "clipped" because excitation of the MLCT transition supplies sufficient energy to evaporate more than the six methanol molecules present in the cluster. "Clipping" of the photoproduct distribution is especially evident in the trace corresponding to excitation with a photon energy of 2.71 eV shown in Figure 5.

For clusters having fewer than six methanol molecules, truncation of the photoproduct distribution and the associated decrease in the width of the photoproduct distribution with increasing photon energy begins at even lower photon energies. Photon energies as low as 2.5 eV remove all of the solvent molecules from $[Fe(bpy)_3 \cdot (CH_3OH)_5]^{2+}$. The average number of solvent molecules lost by $[Fe(bpy)_3 \cdot (CH_3OH)_5]^{2+}$ increases between photon energies of 2.29 and 2.54 eV, where it reaches the maximum possible value of five methanol molecules lost. "Clipping" of the photoproduct ion distributions makes $[Fe(bpy)_3 \cdot (CH_3OH)_6]^{2+}$ the smallest cluster for which an estimate of the average methanol binding energy can be made based on the photon energy dependence of the average number of methanol molecules lost.

The photon energy dependence of the average number of neutrals lost from a photoexcited cluster can be used to find an upper limit for the average binding energy of neutrals in the cluster.[60,61] Unfortunately, determination of the average number of neutrals lost by $[Fe(bpy)_3 \cdot (CH_3OH)_6]^{2+}$ following photoexcitation is limited to a narrow range of energies (2.25−2.41 eV) by the onset energy of MLCT absorption on the low-energy side and truncation of the photoproduct distributions on the high-energy side. Truncated photoproduct distributions overestimate the average neutral binding energy. The values for the average number of neutrals evaporated, which are determined from the integrated areas of the photofragment peaks, range from 4.07 ± 0.27 at 2.25 eV to 4.56 ± 0.16 at 2.41 eV. If one assumes that the *y* intercept of the average number of neutrals lost plotted as a function of photon energy is 0, i.e., no neutrals are lost when photons of zero energy are absorbed, a slope of 1.83(1) eV^{-1} is obtained from the experimental data. This slope yields −0.545 ± 0.034 eV as the upper limit on the average binding energy of the first six methanol molecules to the $[Fe(bpy)_3]^{2+}$ complex. For comparison, the bulk heat of vaporization for methanol is 0.388 eV at 298 K.[57]

Sequential enthalpies of hydration for doubly charged transition-metal ions obtained from gas-phase equilibrium measurements of electrosprayed ions[17] offer benchmarks for comparison of the average binding energy determined from photodissociation of $[Fe(bpy)_3 \cdot (CH_3OH)_6]^{2+}$. Kebarle and co-workers[17] reported sequential binding free energies, $\Delta G°_{n-1,n}$, for the gas-phase hydration equilibria

$$M^{2+} \cdot (H_2O)_{n-1} + H_2O \rightleftarrows M^{2+} \cdot (H_2O)_n \qquad (4)$$

established following electrospray ionization, where M = Mn or Co and $9 \leq n \leq 12$. The values of $\Delta G°_{n-1,n}$, which ranged from −0.31 to −0.37 eV, yielded binding enthalpies of −0.61 to −0.67 eV. At first glance, it may seem inappropriate to compare the average solvent binding energy for a cluster containing a coordination complex as the ionic core, $[Fe(bpy)_3 \cdot (CH_3OH)_6]^{2+}$, with those for clusters consisting of a transition-metal ion with solvent. However, if one assumes octahedral coordination of water molecules around the metal ion, the binding enthalpies reported by Kebarle and co-workers correspond to solvent in the second shell[3] rather than solvent coordinated directly to the metal ion. In $[Fe(bpy)_3 \cdot (CH_3OH)_6]^{2+}$ clusters, methanol molecules are located beyond the primary coordination shell occupied by the bipyridyl ligands. The average binding energy of −0.545 eV for each of the first six methanol molecules associated with $[Fe(bpy)_3]^{2+}$ represents an upper limit because it is based on the assumption that all of the energy deposited in the cluster by excitation of the MLCT transition is used to break bonds, ignoring kinetic energy release[62] and internal excitation of the photofragments. Interactions between second shell solvent and the ionic core are expected to be ion dipole in nature. The weaker binding of second shell methanol molecules in $[Fe(bpy)_3 \cdot (CH_3OH)_n]^{2+}$ clusters relative to second shell water molecules in $M^{2+} \cdot (H_2O)_n$ clusters ($n > 6$) is consistent with the solvent dipole moments,[57] 1.854 D for water vs 1.70 D for methanol. The bulkier bipyridyl ligands in $[Fe(bpy)_3 \cdot (CH_3OH)_6]^{2+}$ clusters should also increase the distance between the metal ion, which serves as the charge center, and the second shell solvent relative to that in $M^{2+} \cdot (H_2O)_n$ clusters, reducing the strength of the ion-dipole interaction. Furthermore, the bulk enthalpies of vaporization for water and methanol at 25 °C (0.456 vs 0.388 eV)[57] indicate stronger interactions between the solvent molecules themselves in bulk water than in bulk methanol, which should be reflected in cluster binding energies beyond the first shell surrounding an ion.

C. Average Internal Energies, Temperatures, and Sequential Binding Energies of $[Fe(bpy)_3 \cdot (CH_3OH)_n]^{2+}$ Clusters. In the development of electrospray ionization for analytical applications, no effort has been made to characterize the internal energies and temperatures of the resulting gas-phase ions, whereas knowledge of the internal temperature becomes an important consideration when ESI is used to prepare molecular ions and clusters for spectroscopic investigation. In fact, the optimized experimental conditions for these two applications of ESI, which have opposing objectives, directly influence the internal temperature of the ions produced. Clusters formed by analyte ions with the electrospray carrier solvent complicate the resulting mass spectra and are typically suppressed in analytical applications through heating or collisional activation, which promote ion desolvation by raising the internal energy of the clusters. In spectroscopic applications, reducing the temperatures of the gas-phase ions can decrease congestion in structured absorption and photofragmentation spectra. Conditions consistent with minimizing the internal energy of ions generated by ESI also favor cluster formation. As described in section II.B, holding both the temperature of the ESI source housing and the kinetic energy of electrosprayed ions as low as possible in the high-pressure regions of the source optimizes cluster formation.

Metastable decomposition of $[Fe(bpy)_3 \cdot (CH_3OH)_n]^{2+}$ clusters between initial mass selection and final detection

$$[Fe(bpy)_3 \cdot (CH_3OH)_n]^{2+} \xrightarrow{k_n(E_n)} [Fe(bpy)_3 \cdot (CH_3OH)_{n-1}]^{2+} + CH_3OH \qquad (5)$$

$$[Fe(bpy)_3 \cdot (CH_3OH)_{n-1}]^{2+} \xrightarrow{k_{n-1}(E_{n-1})} [Fe(bpy)_3 \cdot (CH_3OH)_{n-2}]^{2+} + CH_3OH \qquad (6)$$

$$\vdots$$

allows determination of sequential methanol binding energies and average internal energies using the evaporative ensemble model for unimolecular dissociation of clusters proposed by Klots.[63,64] Conservation of energy dictates for an $[Fe(bpy)_3 \cdot (CH_3OH)_n]^{2+}$ cluster undergoing metastable decomposition that

$$E_{n-1} = E_n - V_n - \epsilon_n \qquad (7)$$

where E_n is the initial internal energy of the cluster, E_{n-1} is the internal energy of the cluster following metastable loss of one methanol molecule, V_n is the binding energy of the *n*th methanol in the cluster, and ϵ_n is the kinetic energy release accompanying metastable loss. The internal energy content of the dissociating species governs unimolecular dissociation rate constants, resulting in $k_n(E_n) > k_{n-1}(E_{n-1})$. The key assumptions in application of the evaporative ensemble model are that cluster evaporation occurs by sequential loss of neutral monomers and that clusters have experienced at least one evaporation event before observation.

In this experiment, cluster ions exit the ESI source at the second skimmer and enter the "collision-free" environs of the mass spectrometer. Ions typically take 5×10^{-5} s to reach the Wien filter, which provides primary mass selection. Loss of one or two neutral methanol molecules (Figure 3) occurs during the $\sim 1.5 \times 10^{-4}$ s transit time of $[Fe(bpy)_3 \cdot (CH_3OH)_n]^{2+}$ clusters, $n = 2-6$, from the Wien filter to the quadrupole mass analyzer. The normalized intensities of metastable decay peaks,[65−67] D_{n-1} and D_{n-2}, defined by

$$D_{n-i} = \frac{I(n-i)}{I(n) + \sum I(n-i)}, \quad i = 1, 2 \tag{8}$$

are used to determine the metastable decay fractions

$$R_{n-i} = \sum_{j=i}^{n} D_{n-j} \tag{9}$$

which are plotted as a function of cluster size in Figure 6a. The definition for metastable decay fractions is based on the premise that loss is sequential; in other words, loss of two neutrals arises from clusters that have previously lost one neutral. The metastable decay fraction corresponding to loss of one solvent molecule, R_{n-1}, ranges from 10.4% for the $n = 2$ cluster to nearly 18.8% for the $n = 6$ cluster. The decay fraction for loss of two methanols, R_{n-2}, increases with cluster size, which is consistent with sequential loss, but remains below 1.3%. The observed increases in the metastable decay fractions with cluster size are characteristic of the evaporative ensemble. As discussed below, it is likely that the observed decay fractions have contributions from collision-induced dissociation[68] in addition to metastable decomposition.

Two different approaches,[65,66,69−71] based on the evaporative ensemble model, have been followed to obtain sequential binding energies from metastable decay fractions for cluster ions generated by multiphoton ionization of neutral clusters. The statistical approach[65,66] uses either Rice−Ramsperger−Kassel (RRK) theory or Rice−Ramsperger−Kassel−Marcus (RRKM) theory to calculate microcanonical rate constants $k(E)$, which depend on binding energies. The rate constants then allow prediction of metastable decay fractions. Binding energies are adjusted until agreement between the calculated and observed decay fractions is reached. A thermodynamic approach[69−71] fits metastable decay fractions to functions of the heat capacity and the Gspann parameter while varying the binding energy.

We follow the statistical approach to estimate sequential solvent binding energies, average cluster internal energies, and cluster temperatures from metastable decomposition of $[Fe(bpy)_3 \cdot (CH_3OH)_n]^{2+}$ clusters. Bréchignac and co-workers[65] first used this approach to determine binding energies for Na_n^+ clusters using RRK theory to find $k_n(E_n)$. Subsequently, Ernstberger et al.[66] applied this method to analyze metastable decomposition of benzene cation clusters using RRKM rate constants. From theory for the evaporative ensemble, the metastable decay fraction is given by

$$R_{n-1} = \frac{\int_0^\infty P_{n-1}(E_{n-1},t_2)\, dE_n}{\int_0^\infty P_n(E_n,t_1)\, dE_n} \tag{10}$$

where

$$P_n(E_n,t_1) = \frac{k_{n+1}}{k_{n+1} - k_n}[\exp(-k_n t_1) - \exp(-k_{n+1} t_1)] \tag{11}$$

is the energy distribution function for the cluster $[Fe(bpy)_3 \cdot (CH_3OH)_n]^{2+}$ at the time of mass selection,

$$P_{n-1}(E_{n-1},t_2) = P_n(E_n,t_1)[1 - \exp(-k_n t_2)] \tag{12}$$

is the energy distribution function for the metastable decay product at the time of mass analysis, t_1 is the time from ion production to mass selection, t_2 is the time from mass selection to mass analysis and detection of metastable decay products, and conservation of energy (eq 7) dictates that E_{n-1} can be expressed as a function of E_n.

We begin our efforts to determine sequential binding energies, average internal energies, and temperatures for $[Fe(bpy)_3 \cdot (CH_3OH)_n]^{2+}$ clusters, $n = 2-6$, with estimation of the rate constants required to evaluate the energy distribution functions and predict metastable decay fractions using RRK theory. As mentioned previously, Bréchignac and co-workers[65] used RRK rate constants for dissociation of Na_n^+ clusters in their implementation of the evaporative ensemble model. Lisy and co-workers[38,40] also utilized an RRK-based approach to successfully model the evaporative decay process and calculate temperatures for $Cs^+ \cdot (CH_3OH)_n$ and $Na^+ \cdot (CH_3OH)_n$ clusters. Uncertainty regarding the intermolecular vibrational frequencies within the clusters prompted Lisy and co-workers to use the RRK model rather than the more rigorous RRKM approach. Levinger[72] used both RRK and RRKM models to predict the internal energies of Ar_n^+ clusters and observed no significant differences in the results provided by the two methods.

From classical RRK theory,[1] the unimolecular dissociation rate constant for $[Fe(bpy)_3 \cdot (CH_3OH)_n]^{2+}$ is given by

$$k_n(E_n) = A\left(\frac{E_n - V_n}{E_n}\right)^{L(n)-1} \tag{13}$$

where A is the frequency prefactor in s^{-1}, E_n is the internal energy of the cluster, V_n is the binding energy of the nth neutral methanol molecule in the cluster, and $L(n)$ is the number of active or effective oscillators in the cluster. Calculation of RRK rate constants for $[Fe(bpy)_3 \cdot (CH_3OH)_n]^{2+}$ requires specification of several variables. In previous RRK modeling of evaporative dissociation from clusters consisting of a metal ion (Cs^+ or Na^+) and methanol molecules, Lisy and co-workers[38,40] set the frequency prefactor, A, at 4×10^{12} s^{-1}. They found that changing the prefactor by a factor of 4 had only a 10% effect on the calculated internal energies.[38] Since the clusters in this study have the same solvent and internal energies are not particularly sensitive to the prefactor, the same value for A is used in calculations for $[Fe(bpy)_3 \cdot (CH_3OH)_n]^{2+}$ clusters.

Selection of an appropriate value for $L(n)$ to evaluate the RRK rate constant for $[Fe(bpy)_3 \cdot (CH_3OH)_n]^{2+}$ clusters presents a challenge because the active oscillators can include not only intermolecular cluster modes but also low-frequency vibrational modes of the $[Fe(bpy)_3]^{2+}$ complex. As a starting point for assigning a reasonable value to $L(n)$, we estimate the number of modes in $[Fe(bpy)_3 \cdot (CH_3OH)_n]^{2+}$ clusters having frequencies below 250 cm^{-1}. At 300 K, 30% of the population for a 250 cm^{-1} vibrational mode is found in excited energy levels. Determination of the number of cluster modes is straightforward; it is simply the difference between the number of vibrational modes in a $[Fe(bpy)_3 \cdot (CH_3OH)_n]^{2+}$ cluster and the sum of the vibrational modes in the isolated $[Fe(bpy)_3]^{2+}$ complex and n CH_3OH molecules, which is $6n$. The difficulty arises in determining the number of low-frequency vibrational modes for the $[Fe(bpy)_3]^{2+}$ complex because a complete normal mode analysis for the tris(2,2′-bipyridyl)iron(II) complex is not available. We estimate that 13 vibrational modes of the tris-(2,2′-bipyridyl)iron(II) complex lie below 250 cm^{-1} based on a partial normal-coordinate analysis of the analogous tris(2,2′-bipyridyl)ruthenium(II) complex,[73,74] a full normal-coordinate analysis of infrared and Raman spectra of the free bipyridyl ligand,[75] and assignments of far-infrared spectra[76] of $[Fe(bpy)_3]^{2+}$. Twelve of these modes are ligand-based, and one is assigned as a N−Fe−N bend.[76] The selection of 250 cm^{-1} as the upper limit for low-frequency modes in our calculations of

TABLE 1: Sequential Solvent Binding Energies, Average Internal Energies, and Temperatures of $[Fe(bpy)_3\cdot(CH_3OH)_n]^{2+}$ Clusters Determined from Measurement of Metastable Decomposition

n	solvent binding energy, V_n, eV	average internal energy, $\bar{E}_n$, eV	cluster temp, K
2	0.516	0.691	321
3	0.513	0.851	319
4	0.462	0.885	277
5	0.438	0.966	261
6	0.405	1.00	239

cluster temperatures permits internal modes of methanol to be neglected. Lisy and co-workers[38,40] took a similar approach in RRK calculations for $Cs^+\cdot(CH_3OH)_n$ and $Na^+\cdot(CH_3OH)_n$ clusters, which yielded temperatures of 241−751 K. The resulting value for the number of low-frequency modes in $[Fe(bpy)_3\cdot(CH_3OH)_n]^{2+}$ clusters is

$$L(n) = 6n + 13 \tag{14}$$

The impact of changing the value of $L(n)$ on sequential binding energies and cluster temperatures will be discussed below because this expression for $L(n)$ may incorrectly estimate the number of effective oscillators for the RRK model. Furthermore, while counting the number of vibrational modes having frequencies below a cutoff value provides a physical context for estimating $L(n)$, the physical significance of this value for $L(n)$ is probably limited. It should also be noted that the RRK model[1] assumes that the $L(n)$ oscillators have the same frequency, which is a reasonable assumption when only intermolecular cluster modes are considered but an oversimplification of the situation in $[Fe(bpy)_3\cdot(CH_3OH)_n]^{2+}$ clusters.

Iterative evaluation of eq 10 using RRK rate constants (eq 13) until agreement is reached between the calculated and observed $n - 1$ metastable decay fractions yields ratios of sequential binding energies, V_{n+1}/V_n. In order to estimate the absolute values of V_n reported in Table 1 and shown in Figure 6b, we set the sequential binding energy for $n = 7$ equal to the bulk heat of vaporization of methanol, 0.388 eV.[57] In $[Fe(bpy)_3\cdot(CH_3OH)_n]^{2+}$ clusters, the coordinated bipyridyl ligands occupy the shell immediately surrounding the iron cation. Methanol solvent molecules occupy the next shell; therefore, it is not unreasonable to assume that as this shell nears completion[77] sequential binding energies will decrease and approach the bulk heat of vaporization.[38,78] In calculations for $Cs^+\cdot(CH_3OH)_n$ clusters, Lisy and co-workers[38] used the bulk value as the binding energy of methanol solvent molecules beyond the first solvation shell. Using the bulk heat of vaporization for the sequential binding energy of the seventh methanol in $[Fe(bpy)_3\cdot(CH_3OH)_n]^{2+}$ clusters may underestimate its value, which would make the sequential binding energies reported for $n = 2-6$ lower limits. If the binding energy of the seventh methanol, V_7, is raised to 0.420 eV, the sequential binding energies for $n < 7$ increase by 0.031−0.042 eV. The photodissociation measurements discussed earlier provide an upper limit of 0.545 ± 0.034 eV on the average methanol binding energy for the first six methanol molecules to $[Fe(bpy)_3]^{2+}$, which neglected the energy carried away by the separating photofragments as translational energy,[62]

$$\epsilon_n = 2(E_n - V_n)/[L(n) - 1] \tag{15}$$

When kinetic energy release is considered, the photodissociation data are consistent with the results from analysis of the metastable decay fractions when V_7 was set at 0.388 eV.

The expression[66]

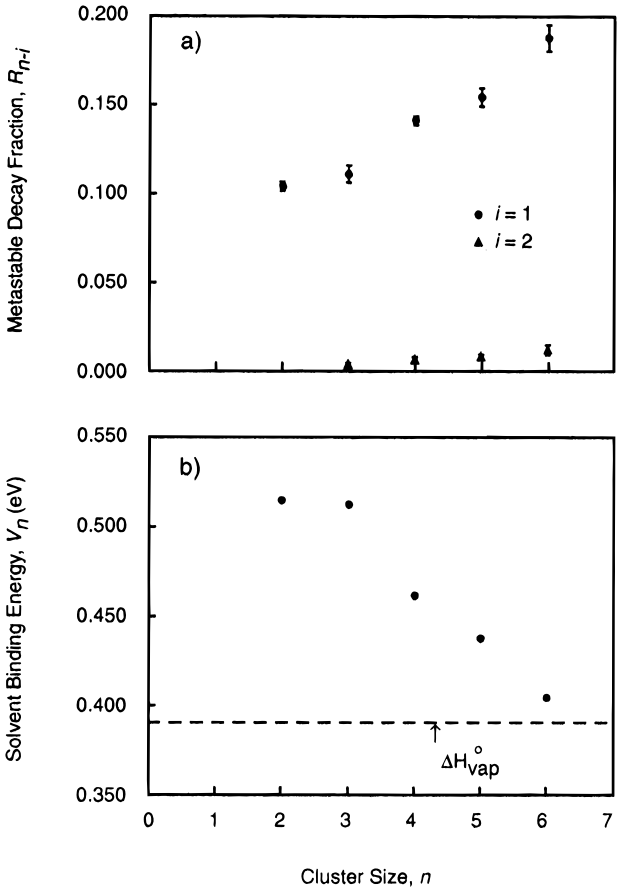

Figure 6. (a) Decay fractions for metastable decomposition of $[Fe(bpy)_3\cdot(CH_3OH)_n]^{2+}$ clusters by sequential loss of methanol solvent molecules. (b) Sequential binding energies of methanol molecules in $[Fe(bpy)_3\cdot(CH_3OH)_n]^{2+}$ clusters determined using the evaporative ensemble model as described in the text.

$$R_{n-2} = \frac{\int_0^\infty P_{n-2}(E_{n-2},t_2)\,dE_n}{\int_0^\infty P_n(E_n,t_1)\,dE_n} \tag{16}$$

for the metastable decay fraction corresponding to loss of two methanol molecules from $[Fe(bpy)_3\cdot(CH_3OH)_n]^{2+}$ clusters developed from the evaporative ensemble model permits prediction of the intensity of the $n - 2$ metastable decay signal relative to the $n - 1$ metastable decay signal. In eq 16,

$$P_{n-2}(E_{n-2},t_2) = P_n(E_n,t_1)\left[1 + \frac{k_{n-1}[\exp(-k_n t_2)] - k_n[\exp(-k_{n-1}t_2)]}{k_n - k_{n-1}}\right] \tag{17}$$

represents the energy distribution function for the $n - 2$ metastable decay product, k_n and k_{n-1} are RRK rate constants calculated using the binding energies, V_n, determined from metastable loss of one methanol molecule, and t_1 corresponds to the time elapsed between ion production and mass selection, while t_2 is the time elapsed between mass selection and detection of metastable decay products. Conservation of energy requires that E_{n-2} is a function of E_n. Comparison of the predictions of the evaporative ensemble model with experimentally-determined metastable decay fractions for loss of two methanol molecules, R_{n-2}, reveals that the measured values are significantly larger. Measured values of R_{n-2} range from 0.3% for $n = 3$ to 1.2% for $n = 6$ as shown in Figure 6a. The evaporative ensemble model predicts decay fractions for loss of two solvent molecules approximately 4 orders of magnitude lower. The measured R_{n-2}

values are consistent with significant contributions from collision-induced dissociation[68] following primary mass selection. As mentioned in section III.A, we estimate that less than 2% of the mass-selected ions collide with background gas as they travel from the mass-selecting Wien filter to the mass-analyzing quadrupole mass filter. Therefore, collision-induced dissociation of the $n - 1$ clusters produced by metastable decay could account for a significant fraction of the $n - 2$ clusters observed.

After sequential binding energies are established, the average internal energy of the evaporative ensemble,

$$\bar{E}_n = \int_0^\infty E_n P_n(E_n,t_1)\, dE_n \qquad (18)$$

can be calculated. Table 1 contains the calculated average internal energies. While the distribution of energies in an evaporative ensemble is not Boltzmann, a "temperature," T, can be determined for purposes of discussion by distributing the average internal energy between the active modes,[38]

$$T_n = E_n/k_B L(n) \qquad (19)$$

where k_B is Boltzmann's constant. The "temperatures" of $[Fe(bpy)_3\cdot(CH_3OH)_n]^{2+}$ clusters (Table 1) range from 321 K for $n = 2$ to 239 K for $n = 6$. If the value of V_7 used in the calculations is raised to 0.420 eV, the cluster temperatures calculated increase by 5−9%.

The uncertainty in counting the number of low-frequency active modes, $L(n)$, prompts us to examine the sensitivity of the binding energies and temperatures reported for $[Fe(bpy)_3\cdot(CH_3OH)_n]^{2+}$ to the value of $L(n)$. The estimate of $6n + 13$ for $L(n)$ is based on the number of intermolecular cluster modes of $[Fe(bpy)_3\cdot(CH_3OH)_n]^{2+}$ and internal modes of $[Fe(bpy)_3]^{2+}$ and methanol having vibrational frequencies below 250 cm^{-1}. If vibrational modes with energies up to 300 cm^{-1} are considered, $L(n)$ becomes $7n + 13$ with addition of the OH twisting mode (ν_8'') at 270 cm^{-1} for each methanol. The calculated sequential binding energies increase by 12% ($n = 6$) to 59% ($n = 2$), and temperatures increase by 15% ($n = 6$) to 64% ($n = 2$) relative to the values calculated for $L(n) = 6n + 13$. Comparison of the sequential binding energies calculated for $L(n) = 7n + 13$ with wavelength-dependent photodissociation data shows that these calculated binding energies are unreasonably high. When excited with a 2.18 eV photon, $[Fe(bpy)_3\cdot(CH_3OH)_6]^{2+}$ clusters lose four methanol molecules on average. Summation of the binding energies determined with $L(n) = 7n + 13$ corresponding to loss of four methanol molecules exceeds the photon energy even before kinetic energy release is considered. Reduction of $L(n)$ to $6n + 9$ yields a sequential binding energy for $n = 2$ that is below the bulk heat of vaporization of methanol and smaller than the values calculated for $n = 3-6$. The temperature determined for $n = 2$ is also smaller than those determined for $n = 3-5$, which are roughly equal. The trends in both sequential binding energies and temperatures calculated for $L(n) = 6n + 9$ are inconsistent with observations in other ionic cluster systems.[38,66,67] Thus, we conclude that the estimate of $6n + 13$ for the number of effective oscillators, $L(n)$, in $[Fe(bpy)_3\cdot(CH_3OH)_n]^{2+}$ is reasonable in the context of the RRK model. Although the assignment of $6n + 13$ as the number of active oscillators was initially guided by physical considerations and is supported by the inconsistency of sequential binding energies obtained using larger and smaller values of $L(n)$ with experimental data, ascribing physical significance to this number is probably not warranted.

These results represent the first effort to characterize the internal temperatures of clusters produced by electrospray ionization. It is evident from these calculations that clusters produced by electrospray ionization are similar in temperature to the $Cs^+\cdot(CH_3OH)_n$ clusters characterized by Lisy and co-workers,[38] which were formed using a thermionic emission ion source. Temperatures for the $Cs^+\cdot(CH_3OH)_n$ clusters were reported to range from 372.4 K for the $n = 3$ clusters to 214.4 K for clusters with $n = 25$.[38] Clusters formed in pulsed expansion cluster ion sources are considerably cooler. Lineberger and co-workers[79] reported temperatures of 20−60 K for $I_2^-(CO_2)_n$ clusters, $n = 0-22$, formed in a pulsed expansion source. Levinger[72] calculated temperatures of 50−59 K for Ar_n^+ clusters, $n = 20-60$, also formed in a pulsed expansion ion source. Both $Cs^+\cdot(CH_3OH)_n$ and $[Fe(bpy)_3\cdot(CH_3OH)_n]^{2+}$ cluster temperatures decrease with increasing cluster size. The effect of this trend on the observed onsets in the gas-phase absorption spectra will be discussed subsequently.

D. Wavelength-Dependent Photofragmentation Spectroscopy of $[Fe(bpy)_3\cdot(CH_3OH)_n]^{2+}$. Excitation of the MLCT transition in $[Fe(bpy)_3\cdot(CH_3OH)_n]^{2+}$ clusters triggers evaporation of several or all of the methanol solvent molecules bound to the coordination complex, providing a convenient method for detecting MLCT absorption. The percentage of the mass-selected $[Fe(bpy)_3\cdot(CH_3OH)_n]^{2+}$ clusters, $n = 2-6$, dissociated by laser excitation was measured as a function of photon energy to indirectly probe the impact of sequential solvation on the MLCT absorption band. Laser-on−laser-off difference mass spectra (Figure 4) offer two ways to quantify photodepletion of the mass-selected parent cluster ion. Integration of the negative-going peaks in laser difference mass spectra directly measures depletion of the parent ion beam. Unfortunately, direct determination of parent cluster ion depletion, which often involves measurement of small changes in a strong signal, can be limited by ion source fluctuations. Summation of the integrated areas of the charged photoproducts provides greater sensitivity because the background signal in the region of the mass spectrum where these ions appear is negligible with the laser blocked. When the measured depletion of the mass-selected cluster ion beam exceeds 10%, the two methods yield equivalent results. Below 10%, direct detection of depletion is less reliable than detection of photoproduct ions in determining the percentage of the mass-selected cluster ion beam that photodissociates. Normalization of the parent depletion signal or photoproduct signal from difference mass spectra with respect to the parent ion intensity in the associated mass spectrum collected with the laser blocked gives the percentage depletion of the mass-selected ion beam accompanying laser excitation.

Figure 7a,b displays percent photodepletion data normalized to 1 W laser power as a function of excitation energy for $[Fe(bpy)_3\cdot(CH_3OH)_n]^{2+}$ clusters, $n = 2-6$. This wavelength range, 530−600 nm, overlaps with the onset region of the MLCT absorption band of $[Fe(bpy)_3]^{2+}$ in methanol solution at room temperature. For clarity, Figure 7a,b presents data obtained with dye laser excitation for clusters containing even ($n = 2, 4, 6$) and odd ($n = 3, 5$) numbers of methanol molecules separately. The percent photodepletion data increase with increasing photon energies over the range studied for the five different clusters ($n = 2-6$), and the onset of these photofragmentation action spectra appears in the same spectral region as the rising red edge of the MLCT band of the $[Fe(bpy)_3]^{2+}$ complex in methanol solution. At photon energies between 1.75×10^4 and 1.89×10^4 cm^{-1}, the fraction of the mass-selected ion beam depleted, normalized with respect to laser power, increases as a function of cluster size when constant overlap between the ion and laser beams is maintained. A maximum in the photodissociation signal is not reached because wave-

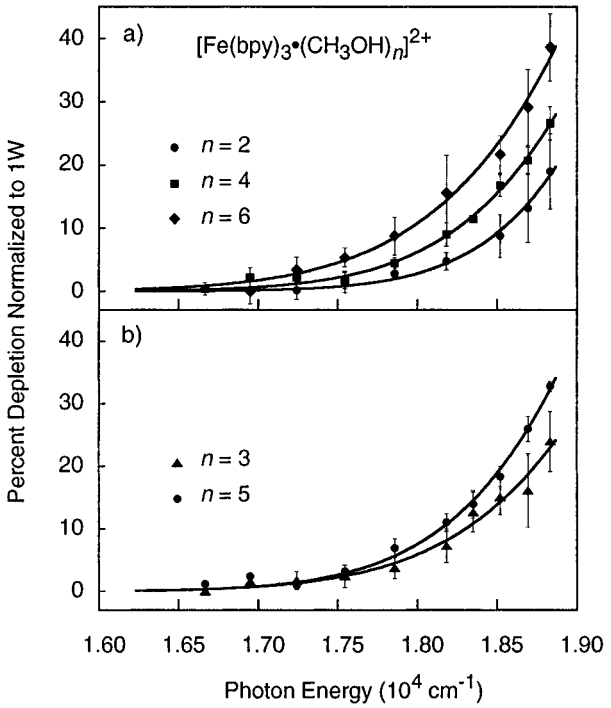

Figure 7. Percent depletion of $[Fe(bpy)_3 \cdot (CH_3OH)_n]^{2+}$ clusters normalized to 1 W laser power plotted as a function of wavelength for (a) $n = 2$, 4, and 6 and (b) $n = 3$ and 5. The percent depletion data, D, determined as a function of photon energy, E, were fit to the trailing edge of a Gaussian function $D = A \exp[-(E - E_{max})^2/(2\sigma^2)]$, where the parameters A, E_{max}, and σ represent the amplitude, maximum, and width, respectively, of the Gaussian function. For reference, the parameters of the fitted Gaussian curves are as follows: $n = 2$, $A = 58.8\%$, $E_{max} = 2.018 \times 10^4$ cm^{-1}, $\sigma = 1.03 \times 10^3$ cm^{-1}; $n = 3$, $A = 50.1\%$, $E_{max} = 2.013 \times 10^4$ cm^{-1}, $\sigma = 1.21 \times 10^3$ cm^{-1}; $n = 4$, $A = 54.3\%$, $E_{max} = 1.998 \times 10^4$ cm^{-1}, $\sigma = 1.11 \times 10^3$ cm^{-1}; $n = 5$, $A = 57.4\%$, $E_{max} = 1.982 \times 10^4$ cm^{-1}, $\sigma = 1.06 \times 10^3$ cm^{-1}; $n = 6$, $A = 54.5\%$, $E_{max} = 1.970 \times 10^4$ cm^{-1}, $\sigma = 1.11 \times 10^3$ cm^{-1}.

lengths bluer than 530 nm are not available from the dye laser with multiline argon ion laser pumping. Although extracavity separation of the output from the multiline argon ion laser provides access to selected bluer wavelengths, spatial mode differences between the dye laser beam and the argon ion beam following extracavity separation prevent meaningful comparison of percent photodepletion data collected using these two different excitation sources. In the absence of data which definitively locate the maxima in the percent depletion signals and establish the amplitude and width of the peak, several possible explanations exist for the differences observed in the wavelength-dependent photofragmentation spectra for clusters having different numbers of methanol molecules associated with the $[Fe(bpy)_3]^{2+}$ complex. The onsets of the photofragmentation action spectra may shift to the red with increasing cluster size. Alternatively, the position of these spectra may remain fixed in energy while the amplitude of the percent depletion signals increases with cluster size as a result of kinetic effects or changes in absorption cross sections.

The appearance of wavelength-dependent photofragmentation of $[Fe(bpy)_3 \cdot (CH_3OH)_n]^{2+}$ clusters in the same spectral region as the condensed phase MLCT absorption band of $[Fe(bpy)_3]^{2+}$ strongly suggests that excitation of the same MLCT transition triggers evaporation of methanol molecules from the clusters. In cluster studies, questions inevitably arise regarding how accurately photofragmentation action spectra reflect absorption spectra, i.e., how efficiently electronic excitation of a chromophore is converted to vibrational excitation of low-frequency intermolecular cluster modes leading to evaporation of neutrals.

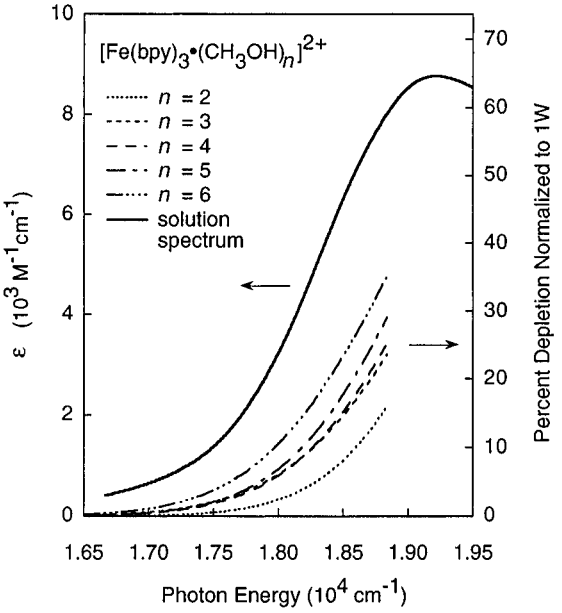

Figure 8. Fitted percent depletion curves for $[Fe(bpy)_3 \cdot (CH_3OH)_n]^{2+}$ clusters, $n = 2-6$, shown with the room temperature (21 °C) absorption spectrum of $Fe(bpy)_3(ClO_4)_2$ in methanol for comparison. The onsets of the photofragmentation spectra shift to the red with the addition of each solvent molecule.

The quantum yield for emission from $[Fe(bpy)_3]^{2+}$ in the condensed phase is sufficiently small that no evidence of radiative relaxation has been detected,[44] which is consistent with efficient conversion of electronic excitation to internal excitation. Photon energies of 2.07−2.34 eV are more than sufficient to cause loss of loosely bound solvent molecules on the time scale of our experiment. The RRK rate constants for loss of the first methanol molecule exceed 1×10^9 s^{-1} for $[Fe(bpy)_3 \cdot (CH_3OH)_n]^{2+}$ cluster sizes $n = 2-6$ (section III.C). These rate constants also decrease with increasing cluster size, which would result in a reduction rather than an increase in the intensity of the percent depletion signal with increasing cluster size. As a consequence, we rule out cluster size-dependent kinetics as the origin of the observed differences in the wavelength-dependent photofragmentation spectra.

The relationship between absorption and cluster photodissociation can be examined quantitatively by comparing the measured depletion of the parent ion beam with that predicted using the molar absorptivity of $[Fe(bpy)_3]^{2+}$ in methanol solution (Figure 8). Assuming a photofragmentation quantum yield of unity and complete overlap of the laser with the ion beam, we predict 70% depletion of the mass-selected cluster at a laser fluence of 68 W cm^{-2} (0.3 W, 0.75 mm beam diameter) using the solution molar absorptivity at 530 nm. The observed 15% depletion of $[Fe(bpy)_3 \cdot (CH_3OH)_6]^{2+}$ clusters at 530 nm is lower than the predicted depletion, but within half an order of magnitude. One possible explanation for the lower measured depletion is less than complete overlap of the ion beam with the laser beam. Furthermore, the photofragmentation action spectra in Figure 7a,b appear to either shift to the red or increase in amplitude with increasing solvation. Based on this trend, the molar absorptivity of $[Fe(bpy)_3]^{2+}$ in solution will overestimate the absorption of all clusters at this wavelength. Further discussion of the relationship between the solution absorption spectrum and cluster photofragmentation action spectra is found below.

Limitations in the laser system used in this study prevent location of the maxima in the wavelength-dependent photodissociation spectra of $[Fe(bpy)_3 \cdot (CH_3OH)_n]^{2+}$ to allow direct

comparison of the solution and gas-phase cluster spectra. However, in previous work,[42] we estimated the shift in the maximum of the MLCT band for $[Fe(bpy)_3 \cdot (CH_3OH)_6]^{2+}$ clusters relative to that for $[Fe(bpy)_3]^{2+}$ in solution using the ratios of photodepletion for $[Fe(bpy)_3 \cdot (CH_3OH)_6]^{2+}$ to that for $[Ru(bpy)_3 \cdot (CH_3OH)_6]^{2+}$ at four wavelengths between 458 and 514 nm. Comparison of the cluster photodestruction ratios with solution molar absorptivity ratios yields a shift to the blue of approximately 540 cm^{-1} in going from solution to the partially solvated $[Fe(bpy)_3 \cdot (CH_3OH)_6]^{2+}$ clusters. This value is based on the assumption that the shape of the gas-phase absorption band is the same as that observed in the condensed phase and that the shifts of the $[Ru(bpy)_3]^{2+}$ and $[Fe(bpy)_3]^{2+}$ spectra are approximately the same; as a consequence, the shift of 540 cm^{-1} should be considered a rough estimate.

Wavelength-dependent photofragmentation data for $[Fe(bpy)_3 \cdot (CH_3OH)_6]^{2+}$ were fit to a Gaussian curve with its maximum shifted by +540 cm^{-1} with respect to the maximum of the solution absorption spectrum to permit comparison with the solution spectrum. Data points in the photofragmentation action spectra for $[Fe(bpy)_3 \cdot (CH_3OH)_n]^{2+}$ clusters, $n = 2-5$, were then fit to Gaussian curves while varying one or two parameters (maximum, width, and amplitude) and holding the remaining parameter(s) fixed at the values obtained for $[Fe(bpy)_3 \cdot (CH_3OH)_6]^{2+}$. The data for clusters with $n = 2-5$ were also fit to Gaussian functions having the same area as the Gaussian for the $n = 6$ data. The poorest fits were obtained when the amplitude or both the amplitude and peak maximum were allowed to vary, as determined from the sum of χ^2 values for $[Fe(bpy)_3 \cdot (CH_3OH)_n]^{2+}$ clusters, $n = 2-5$. The fits when the area, width, or amplitude were fixed yielded the lowest χ^2 values and essentially indistinguishable fits.

We cannot totally eliminate a change in the amplitude of a spectral feature whose maximum and width remain fixed while the extent of solvation of the $[Fe(bpy)_3]^{2+}$ complex is varied as a possible explanation for the observed differences in the percent depletion spectra of $[Fe(bpy)_3 \cdot (CH_3OH)_n]^{2+}$ clusters. However, we favor a red shift of the onset of the MLCT absorption band with increasing cluster size as a more likely interpretation of the data shown in Figure 7a,b for several reasons. In bulk solution the maximum of the MLCT absorption band shifts with solvent, but the area remains essentially unchanged, which is consistent with a constant oscillator strength and no change in chromophore. We anticipate that adding one methanol molecule to $[Fe(bpy)_3 \cdot (CH_3OH)_n]^{2+}$ clusters will have an even smaller effect on absorption by the $[Fe(bpy)_3]^{2+}$ chromophore than changing the solvent in the condensed phase. Preliminary results in an investigation of the effect of sequential solvation on the related iron(II)−polypyridine complex bis(2,2′,2″-terpyridyl)-iron(II) indicate that while widths and maxima of MLCT absorption features detected using photofragmentation change as a function of solvent number and type, the area of the observed MLCT band is roughly conserved.[49] Finally, poorest agreement between experimental data and fitted Gaussian functions is obtained when the amplitude was permitted to vary while holding the position and width fixed. There is also no evidence for radiative decay[44] of the excited state prepared by excitation of the MLCT transition in $[Fe(bpy)_3]^{2+}$ that would influence the photodissociation yield. Previously, we ruled out kinetic effects as an explanation for the observed cluster size dependence of the percent depletion spectra.

Figure 7a,b shows the experimental data and the fitted curves corresponding to a fixed area. Comparable fits were obtained by fixing the Gaussian width or amplitude. The primary purpose of the fitted curves in Figure 7a,b is to summarize the experimental data. Figure 8 displays the portions of the fitted curves that overlap with the photofragmentation data collected for $[Fe(bpy)_3 \cdot (CH_3OH)_n]^{2+}$ clusters, $n = 2-6$, and the room temperature absorption spectrum of $[Fe(bpy)_3]^{2+}$ in methanol. The solution spectrum and fitted curve for $[Fe(bpy)_3 \cdot (CH_3OH)_6]^{2+}$ were normalized with respect to peak maxima for purposes of comparison.

Figure 8 shows that the onsets in the MLCT transition shift to the red as methanol solvent molecules are added sequentially to the microsolvent environment surrounding the $[Fe(bpy)_3]^{2+}$ complex, which is consistent with preferential solvation of the excited electronic state relative to the ground state. With six methanol molecules, the red edge of the cluster percent depletion spectrum remains significantly shifted from the bulk absorption spectrum. At 530 nm, the spectral shift in the cluster environment reduces absorption by $[Fe(bpy)_3]^{2+}$ in the $n = 6$ cluster by a factor of 2 relative to solution. The observed shift in the absorption onset does not simply reflect temperature variations between clusters of different sizes. As discussed earlier, the cluster temperatures decrease with increasing cluster size. If the shift in the onset of the MLCT transition is due solely to variations in the temperature of the gas-phase clusters, increasing solvation will shift the MLCT transition to the blue rather than to the red.

Finally, we have reported the metastable decomposition of $[Fe(bpy)_3 \cdot (CH_3OH)_n]^{2+}$ clusters to form $[Fe(bpy)_3 \cdot (CH_3OH)_{n-1}]^{2+}$ between initial mass selection and final mass analysis (section III.C). Photofragmentation of the $n - 1$ clusters observed in the laser difference mass spectra (Figure 4) contributes to the intensity of the observed photofragment peaks. The $n - 1$ peak generally accounts for 10−20% of the total ion signal observed with the laser off. In cases where percent depletion could be reliably determined from both parent cluster depletion and photoproduct ion signal, the estimated contribution from the $n - 1$ cluster ion fell within the experimental error between the two methods. At a given excitation energy on the rising edge of the cluster MLCT band, the percent depletion of $[Fe(bpy)_3 \cdot (CH_3OH)_{n-1}]^{2+}$ and resulting contribution to the photoproduct ion signal are smaller than those of the mass-selected $[Fe(bpy)_3 \cdot (CH_3OH)_n]^{2+}$ cluster. Consequently, no correction was made to the percent depletion data for the contribution of $[Fe(bpy)_3 \cdot (CH_3OH)_{n-1}]^{2+}$ photodissociation to the photoproduct ion signal. The net effect of no correction for the presence of metastable decay products may be a slight red shift of the reported MLCT bands with respect to their actual positions.

IV. Conclusions

We have reported the first effort to utilize electrospray ionization to produce divalent gas-phase coordination complexes with attached solvent molecules to probe the influence of solvent−solute interactions on the energetics of photoinitiated charge transfer. Electrospray ionization produces gas-phase clusters containing transition-metal ions in the +2 oxidation state in concentrations which are sufficient for subsequent spectroscopic analysis. Observation of the onset of photoinitiated MLCT in $[Fe(bpy)_3 \cdot (CH_3OH)_n]^{2+}$ shows that transition-metal complexes isolated in these gas-phase clusters are analogous to the species present in solution and may serve as useful models for investigating ion−solvent interactions in the bulk solution. In addition, metastable decomposition of clusters following primary mass selection permits determination of sequential binding energies and characterization of the internal temperatures of clusters generated by ESI.

Acknowledgment. Support from Research Corporation (Cottrell Scholar Award), the National Science Foundation (CHE-9119553), the ACS Petroleum Research Fund (ACS-PRF 24867-G6), and Vanderbilt University is gratefully acknowledged. G.B.G. was supported by an ACS−PRF Undergraduate Research Supplement and a Stephen Harris Cook Memorial Fellowship (Vanderbilt University).

References and Notes

(1) Steinfeld, J. I.; Francisco, J. S.; Hase, W. L. *Chemical Kinetics and Dynamics*; Prentice-Hall: Englewood Cliffs, NJ, 1989; pp 156−171, 358−361, 402−414.
(2) Olmstead, W. N.; Brauman, J. I. *J. Am. Chem. Soc.* **1977**, *99*, 4219.
(3) Frank, H. S.; Wen, W.-Y. *Discuss. Faraday Soc.* **1957**, *24*, 133.
(4) Castleman, A. W., Jr.; Keesee, R. G. *Acc. Chem. Res.* **1986**, *19*, 413.
(5) Bieske, E. J.; Maier, J. P. *Chem. Rev.* **1993**, *93*, 2603.
(6) Roth, L. M.; Freiser, B. S. *Mass Spectrom. Rev.* **1991**, *10*, 303.
(7) Tonkyn, R.; Weisshaar, J. C. *J. Am. Chem. Soc.* **1986**, *108*, 7128.
(8) Gord, J. R.; Freiser, B. S.; Buckner, S. W. *J. Phys. Chem.* **1991**, *95*, 8274.
(9) Ranasinghe, Y. A.; MacMahon, T. J.; Freiser, B. S. *J. Phys. Chem.* **1991**, *95*, 7721.
(10) Gord, J. R.; Freiser, B. S.; Buckner, S. W. *J. Chem. Phys.* **1989**, *91*, 7530.
(11) Hill, Y. D.; Freiser, B. S.; Bauschlicher, C. W., Jr. *J. Am. Chem. Soc.* **1991**, *113*, 1507.
(12) Fenn, J. B.; Mann, M.; Meng, C. K.; Wong, S. G.; Whitehouse, C. M. *Mass Spectrom. Rev.* **1990**, *9*, 37.
(13) Woodward, C. A.; Dobson, M. P.; Stace, A. J. *J. Phys. Chem.* **1996**, *100*, 5605.
(14) Dobson, M. P.; Stace, A. J. *J. Chem. Soc., Chem. Commun.* **1996**, 1533.
(15) Blades, A. T.; Jayaweera, P.; Ikonomou, M. G.; Kebarle, P. *Int. J. Mass Spectrom. Ion Processes* **1990**, *102*, 251.
(16) Blades, A. T.; Ikonomou, M. G.; Kebarle, P. *Anal. Chem.* **1991**, *63*, 2109.
(17) Blades, A. T.; Jayaweera, P.; Ikonomou, M. G.; Kebarle, P. *J. Chem. Phys.* **1990**, *92*, 5900.
(18) Katta, V.; Chowdhury, S. K.; Chait, B. T. *J. Am. Chem. Soc.* **1990**, *112*, 5348.
(19) Arakawa, R.; Matsuo, T.; Ito, H.; Katakuse, I.; Nozaki, K.; Ohno, T.; Haga, M. *Org. Mass Spectrom.* **1994**, *29*, 289.
(20) Andersen, U. N.; McKenzie, C. J.; Bojesen, G. *Inorg. Chem.* **1995**, *34*, 1435.
(21) Lessen, D.; Brucat, P. J. *J. Chem. Phys.* **1989**, *90*, 6296.
(22) Lessen, D.; Brucat, P. J. *J. Chem. Phys.* **1989**, *91*, 4522.
(23) Asher, R. L.; Bellert, D.; Buthelezi, T.; Brucat, P. J. *Chem. Phys. Lett.* **1994**, *227*, 277.
(24) Asher, R. L.; Bellert, D.; Buthelezi, T.; Brucat, P. J. *Chem. Phys. Lett.* **1994**, *228*, 599.
(25) Asher, R. L.; Bellert, D.; Buthelezi, T.; Lessen, D.; Brucat, P. J. *Chem. Phys. Lett.* **1995**, *234*, 119.
(26) Lessen, D. E.; Asher, R. L.; Brucat, P. J. *J. Chem. Phys.* **1991**, *95*, 1414.
(27) Asher, R. L.; Bellert, D.; Buthelezi, T.; Weerasekera, G.; Brucat, P. J. *Chem. Phys. Lett.* **1994**, *228*, 390.
(28) Asher, R. L.; Bellert, D.; Buthelezi, T.; Brucat, P. J. *Chem. Phys. Lett.* **1994**, *227*, 623.
(29) Lessen, D. E.; Asher, R. L.; Brucat, P. J. *J. Chem. Phys.* **1990**, *93*, 6102.
(30) Pilgrim, J. S.; Yeh, C. S.; Duncan, M. A. *Chem. Phys. Lett.* **1993**, *210*, 322.
(31) Pilgrim, J. S.; Yeh, C. S.; Berry, K. R.; Duncan, M. A. *J. Chem. Phys.* **1994**, *100*, 7945.
(32) Willey, K. F.; Yeh, C. S.; Robbins, D. L.; Pilgrim, J. S.; Duncan, M. A. *J. Chem. Phys.* **1992**, *97*, 8886.
(33) Yeh, C. S.; Willey, K. F.; Robbins, D. L.; Pilgrim, J. S.; Duncan, M. A. *Chem. Phys. Lett.* **1992**, *196*, 233.
(34) Yeh, C. S.; Willey, K. F.; Robbins, D. L.; Pilgrim, J. S.; Duncan, M. A. *J. Chem. Phys.* **1993**, *98*, 1867.
(35) Willey, K. F.; Cheng, P. Y.; Bishop, M. B.; Duncan, M. A. *J. Am. Chem. Soc.* **1991**, *113*, 4721.
(36) Shen, M. H.; Farrar, J. M. *J. Phys. Chem.* **1989**, *93*, 4386.
(37) Shen, M. H.; Winniczek, J. W.; Farrar, J. M. *J. Phys. Chem.* **1987**, *91*, 6447.
(38) Draves, J. A.; Luthey-Schulten, Z.; Liu, W.-L.; Lisy, J. M. *J. Chem. Phys.* **1990**, *93*, 4589.
(39) Liu, W.-L.; Lisy, J. M. *J. Chem. Phys.* **1988**, *89*, 605.
(40) Selegue, T. J.; Moe, N.; Draves, J. A.; Lisy, J. M. *J. Chem. Phys.* **1992**, *96*, 7268.
(41) Willey, K. F.; Yeh, C. S.; Robbins, D. L.; Duncan, M. A. *J. Phys. Chem.* **1992**, *96*, 9106.
(42) Burns, T. D.; Spence, T. G.; Mooney, M. A.; Posey, L. A. *Chem. Phys. Lett.* **1996**, *258*, 669.
(43) Bryant, G. M.; Fergusson, J. E.; Powell, H. K. J. *Aust. J. Chem.* **1971**, *24*, 257.
(44) Hauser, A. *Chem. Phys. Lett.* **1990**, *173*, 507.
(45) Allen, M. H.; Vestal, M. L. *J. Am. Soc. Mass Spectrom.* **1992**, *3*, 18.
(46) Chowdhury, S. K.; Katta, V.; Chait, B. T. *Rapid Commun. Mass Spectrom.* **1990**, *4*, 81.
(47) Yamashita, M.; Fenn, J. B. *J. Phys. Chem.* **1984**, *88*, 4451.
(48) O'Hanlon, J. F. *A User's Guide to Vacuum Technology*, 2nd ed.; John Wiley and Sons: New York, 1989; p 26.
(49) Burns, T. D. Ph.D. Dissertation, Vanderbilt University, 1997.
(50) Wåhlin, L. *Nucl. Instrum. Meth.* **1964**, *27*, 55.
(51) Seliger, R. L. *J. Appl. Phys.* **1972**, *43*, 2352.
(52) Zeman, H. D. *Rev. Sci. Instrum.* **1977**, *48*, 1079.
(53) Farley, J. W. *Rev. Sci. Instrum.* **1985**, *56*, 1834.
(54) Klemperer, O.; Barnett, M. E. *Electron Optics*, 3rd ed.; Cambridge University Press: Cambridge, 1971; pp 11−12, 80.
(55) Ervin, K. M. Ph.D. Dissertation, University of California, Berkeley, 1986.
(56) Fork, R. L. *Opt. Lett.* **1986**, *11*, 629.
(57) Lide, D. R. *Handbook of Chemistry and Physics*, 71st ed.; CRC Press: Boca Raton, FL, 1990; pp 6-117, 9-44, 9-46, 11-47−11-48.
(58) Draves, J. A.; Lisy, J. M. *J. Am. Chem. Soc.* **1990**, *112*, 9006.
(59) Spence, T. G.; Burns, T. D.; Posey, L. A. *J. Phys. Chem.*, in press.
(60) Alexander, M. L.; Johnson, M. A.; Lineberger, W. C. *J. Chem. Phys.* **1985**, *82*, 5288.
(61) Alexander, M. L.; Johnson, M. A.; Levinger, N. E.; Lineberger, W. C. *Phys. Rev. Lett.* **1986**, *57*, 976.
(62) Engelking, P. C. *J. Chem. Phys.* **1986**, *85*, 3103.
(63) Klots, C. E. *Z. Phys. D* **1987**, *5*, 83.
(64) Klots, C. E. *J. Phys. Chem.* **1988**, *92*, 5864.
(65) Bréchignac, C.; Cahuzac, Ph.; Leygnier, J.; Weiner, J. *J. Chem. Phys.* **1989**, *90*, 1492.
(66) Ernstberger, B.; Krause, H.; Neusser, H. J. *Ber. Bunsenges. Phys. Chem.* **1993**, *97*, 884.
(67) Wei, S.; Tzeng, W. B.; Castleman, A. W., Jr. *J. Chem. Phys.* **1990**, *93*, 2506.
(68) Stace, A. J.; Lethbridge, P. G.; Upham, J. E.; Wright, M. *J. Chem. Phys.* **1988**, *88*, 483.
(69) Klots, C. E. *Z. Phys. D* **1991**, *21*, 335.
(70) Wei, S.; Kilgore, K.; Tzeng, W. B.; Castleman, A. W., Jr. *J. Phys. Chem.* **1991**, *95*, 8306.
(71) Wei, S.; Shi, Z.; Castleman, A. W., Jr. *J. Chem. Phys.* **1991**, *94*, 8604.
(72) Levinger, N. E. Ph.D. Dissertation, University of Colorado at Boulder, 1990.
(73) Strommen, D. P.; Mallick, P. K.; Danzer, G. D.; Lumpkin, R. S.; Kincaid, J. R. *J. Phys. Chem.* **1990**, *94*, 1357.
(74) Mallick, P. K.; Danzer, G. D.; Strommen, D. P.; Kincaid, J. R. *J. Phys. Chem.* **1988**, *92*, 5628.
(75) Neto, N.; Muniz-Miranda, M.; Angeloni, L.; Castellucci, E. *Spectrochim. Acta* **1983**, *39A*, 97.
(76) Hutchinson, B.; Takemoto, J.; Nakamoto, K. *J. Am. Chem. Soc.* **1970**, *92*, 3335.
(77) Kurucsev, T.; Sargeson, A. M.; West, B. O. *J. Phys. Chem.* **1957**, *61*, 1567.
(78) Castleman, A. W., Jr.; Keesee, R. G. *Chem. Rev.* **1986**, *86*, 589.
(79) Papanikolas, J. M.; Gord, J. R.; Levinger, N. E.; Ray, D.; Vorsa, V.; Lineberger, W. C. *J. Phys. Chem.* **1991**, *95*, 8028.